nature COMMUNICATIONS

ARTICLE

Received 3 Dec 2014 | Accepted 5 May 2015 | Published 11 Jun 2015 DOI: 10.1038/ncomms8426 OPEN

Induced superconductivity in high-mobility two-dimensional electron gas in gallium arsenide heterostructures

Zhong Wan[1], Aleksandr Kazakov[1], Michael J. Manfra[1,2,3,4], Loren N. Pfeiffer[5], Ken W. West[5] & Leonid P. Rokhinson[1,2,4]

Search for Majorana fermions renewed interest in semiconductor–superconductor interfaces, while a quest for higher-order non-Abelian excitations demands formation of superconducting contacts to materials with fractionalized excitations, such as a two-dimensional electron gas in a fractional quantum Hall regime. Here we report induced superconductivity in high-mobility two-dimensional electron gas in gallium arsenide heterostructures and development of highly transparent semiconductor–superconductor ohmic contacts. Supercurrent with characteristic temperature dependence of a ballistic junction has been observed across 0.6 μm, a regime previously achieved only in point contacts but essential to the formation of well separated non-Abelian states. High critical fields (>16 T) in NbN contacts enables investigation of an interplay between superconductivity and strongly correlated states in a two-dimensional electron gas at high magnetic fields.

[1] Department of Physics and Astronomy, Purdue University, West Lafayette, Indiana 47907, USA. [2] Department of Electrical Engineering, Purdue University, West Lafayette, Indiana 47907, USA. [3] Department of Materials Engineering, Purdue University, West Lafayette, Indiana 47907, USA. [4] Birck Nanotechnology Center, Purdue University, West Lafayette, Indiana 47907, USA. [5] Department of Electrical Engineering, Princeton University, Princeton, New Jersey 08544, USA. Correspondence and requests for materials should be addressed to L.P.R. (email: leonid@purdue.edu).

Introduction of Josephson field effect transistor concept[1] sparked active research on proximity effects in semiconductors. Induced superconductivity and electrostatic control of critical current has been demonstrated in two-dimensional gases in InAs[2,3], graphene[4] and topological insulators[5–8], and in one-dimensional systems[9–11] including quantum spin Hall edges[12,13]. Recently, interest in superconductor–semiconductor interfaces was renewed by the search for Majorana fermions[14,15], which were predicted to reside at the interface[16–18]. More exotic non-Abelian excitations, such as parafermions (fractional Majorana fermions)[19–21] or Fibonacci fermions may be formed when fractional quantum Hall edge states interface with superconductivity. Realization of a long-sought regime of an interplay between superconductivity and strongly correlated states in a two-dimensional electron gas (2DEG) at high magnetic fields[22–27] requires development of transparent superconducting contacts to high-mobility 2DEG, which remain superconducting at high magnetic fields.

Proximity effects in GaAs quantum wells have been intensively investigated in the past and Andreev reflection has been observed by several groups[28–31]. Unlike in InAs, where Fermi level (E_F) at the surface resides in the conduction band, in GaAs E_F is pinned in the middle of the gap, which results in a high Schottky barrier between a 2DEG and a superconductor and low transparency non-ohmic contacts. Heavy doping can move E_F into the conduction band and, indeed, superconductivity has been induced in heavily doped bulk n^{++} GaAs[32]. In quantum wells, similar results were obtained by annealing indium contacts[33]; however, the critical field of indium is ~ 30 mT, well below the fields required to form quantum Hall effect (QHE) states.

In this article, we report the development of transparent superconducting ohmic contacts to high-mobility 2DEG in GaAs. The superconducting contact is type-II NbN with large critical field >16 T. Induced superconductivity is observed across 1.6 µm of a 2D gas at zero field. From temperature dependence of the critical current and analysis of Andreev reflection, we estimate contact transparency parameter $Z \lessapprox 0.2$. Induced superconductivity is observed in magnetic fields up to 0.2 T. At high magnetic fields, we observe deviations of longitudinal and Hall resistances from a similar data obtained with normal contacts, a clear indication of an interplay between superconductivity and QHE edge states.

Results

Heterostructures design. In conventional quantum well structures AlGaAs, barrier between 2DEG and the surface of the sample adds an extra 0.3 eV to the Schottky barrier when contacts are defused from the top. We alleviated these problems by growing an inverted heterojunction structures, where a 2DEG resides at the GaAs/AlGaAs interface but the AlGaAs barrier with modulation doping is placed below the 2DEG, see Fig. 1b, where band diagram was calculated using a self-consistent Poisson solver[34] (The program can be downloaded from http://www3.nd.edu/~gsnider/). Contacts are recessed into the top GaAs layer to bring the superconductor closer to the 2DEG. A thin layer of AuGe and NbN superconductor form low resistance ohmic contacts to the 2DEG after annealing. The inverted heterostructure increases the contact area of side contacts compared with quantum well structures by utilizing all GaAs layer above the heterointerface for carrier injection (130 nm in our inverted heterostructure versus 20–30 nm in typical quantum wells, see Supplementary Fig. 1 and Supplementary Note 1).

Induced superconductivity. We report induced superconductivity in two devices from different wafers. Sample A has long (70 µm) contacts separated by 1.6 µm of 2DEG, contacts to sample B are formed to the edge of a mesa with 0.6 µm separation, see Fig. 1a. Details of device fabrication are described in Methods. When cooled down to 4 K in the dark, both the samples show resistance in excess of 1 MΩ. After illumination with red light-emitting diode a 2DEG is formed and 2-terminal resistance drops to $<500\,\Omega$. As shown in Fig. 1d, sample resistance RB_{3-4} gradually decreases on cooldown from 4 K to the base temperature and the superconductor–2DEG–superconductor (S–2DEG–S) junction becomes superconducting at $T_c \sim 0.3$ K.

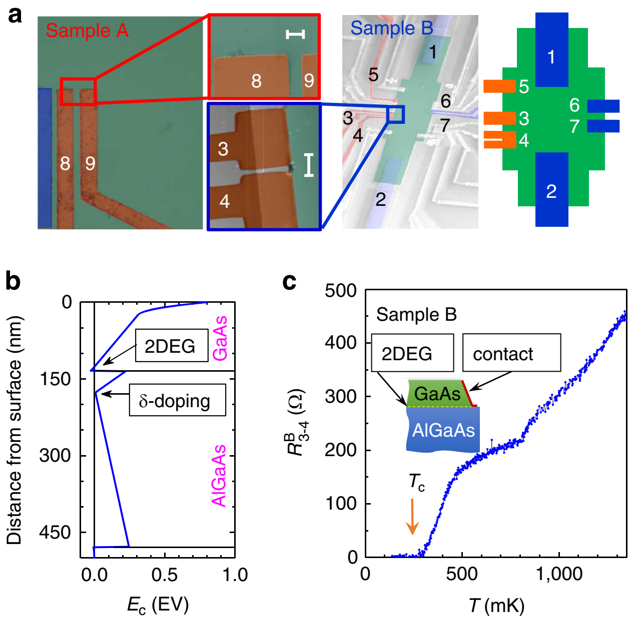

Figure 1 | Design and superconducting transition. (**a**) Scanning electron microscope images of test devices similar to samples A and B. Enlarged region for sample B is an atomic force microscope image of a real sample. 2D gas regions are false-colour coded with green, superconducting and normal contacts are coded with orange and blue, respectively. Scale bar is 2 µm. (**b**) Simulation of the conduction band energy profile in the heterostructure. (**c**) T-dependence of resistance between contacts 3 and 4 in sample B measured with 10 nA a.c. excitation. Superconducting transition is observed at $T_c \approx 290$ mK.

Voltage–current $V(I)$ characteristics for two S–2DEG–S junctions (between contacts 8 and 9 for sample A, and 3 and 4 for sample B) are shown in Fig. 2. Both the samples show zero-resistance state at small currents with abrupt switching into resistive state at critical currents $I_c = 0.22$ and 0.23 µA for samples A and B, respectively. We attribute hysteresis in $V(I)$ characteristics to Joule heating in the normal state.

The most attractive property of a high-mobility 2DEG is large mean free path $l \gg \xi_0$, with $l = 24$ µm and the Bardeen-Cooper-Schrieffer (BCS) coherence length $\xi_0 = \hbar v_F/\pi\Delta = 0.72$ µm for sample B. Here $v_F = \hbar\sqrt{2\pi n}/m$ is the Fermi velocity, n is a 2D gas density, m is an effective mass and $\Delta = 1.76 k_B T_c = 46$ µeV is the induced superconducting gap. Evolution of $V(I)$ with T is shown in Fig. 3a. Experimentally obtained T-dependence of I_c is best described by the Kulik–Omelyanchuk theory for ballistic junctions ($L \ll l$) (ref. 35), the blue curve in Fig. 3b. For comparison, we also plot $I_c(T)$ dependence for the dirty limit $L \ll \sqrt{l\xi_0}$ (ref. 36), which exhibits characteristic saturation of I_c at low temperatures.

In short ballistic junctions, $L \ll \xi_0 \ll l$ the product $I_c(0)RN = \pi\Delta/e$ does not depend on the junction length L. For $L \sim \xi_0$ this product is reduced by a factor $2\xi_0/(L + 2\xi_0)$ (ref. 37). The

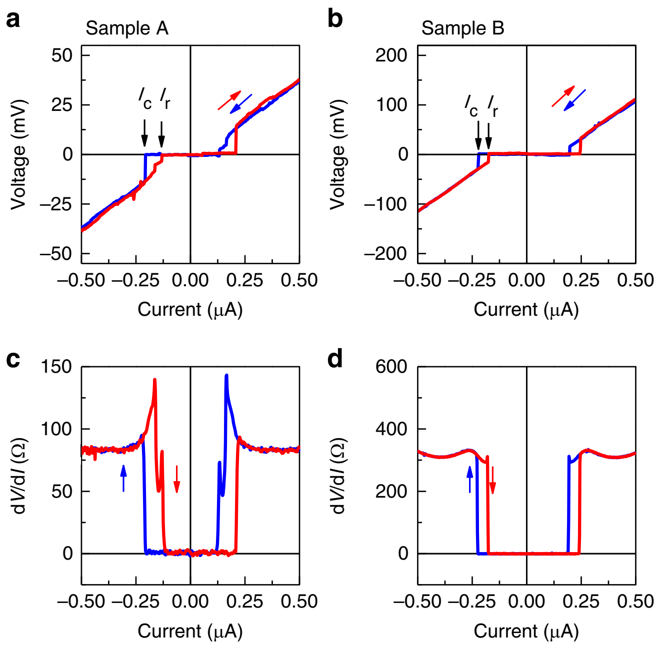

Figure 2 | Induced superconductivity in a high-mobility 2D electron gas in GaAs. Voltage-current characteristics (**a**,**b**) and differential resistance (**c**,**d**) for samples A (**a**,**c**) and B (**b**,**d**). The conduction is measured between contacts (8-9) for sample A and (3-4) for sample B. dV/dI is measured with $I_{a.c.}=1$ nA. Induced superconductivity with zero voltage is observed with critical currents $I_c\sim 220$ nA for sample A and $I_c\sim 230$ for sample B. Red (blue) traces are for current increasing (decreasing).

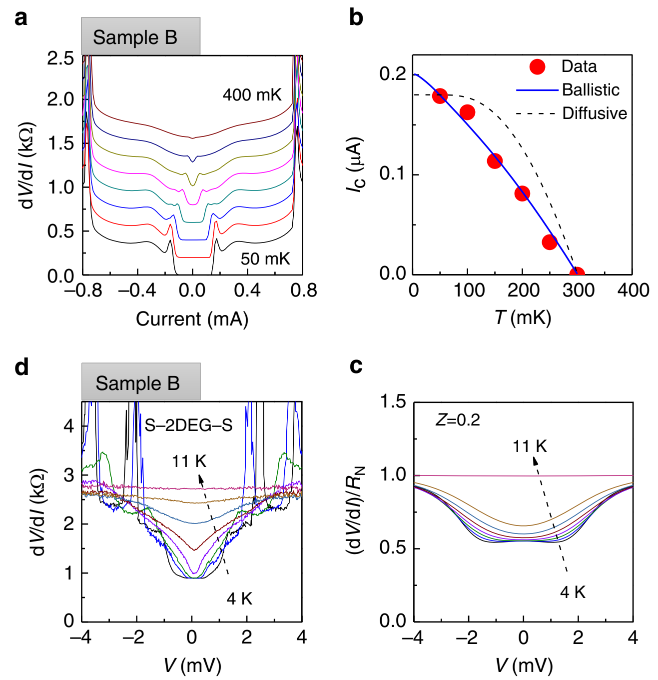

Figure 3 | Temperature dependence of superconductivity in a ballistic junction. (**a**) Evolution of the induced superconductivity with T for sample B. The $R(I)$ curves are offset proportional to T for $T>50$ mK. (**b**) Temperature dependence of critical current $I_c(T)$ is extracted from (**a**) and compared with the expected T-dependence for ballistic and diffusive regimes (reduced I_c compared with Fig. 2 is due to larger $I_{a.c.}=10$ nA used in this experiment). (**c**) High-temperature data shows Andreev reflection (excess current and reduced dV/dI around $V=0$. The curves are not offset. In **d**, excess current is modelled within the Blonder–Tinkham–Klapwijk theory[39] with $Z=0.2$.

measured $I_cRN=83\,\mu$V for sample B is in a good agreement with an estimate $\pi\Delta/e\cdot 2\xi_0/(L+2\xi_0)=90\,\mu$V. For sample A, the $I_cRN=19\,\mu$V while the estimated product is $\approx 50\,\mu$V. The reduction is consistent with the geometry of sample A, where a region of the 2DEG with induced superconductivity is shunted by a large region of a 2DEG in a normal state.

Transparency of a superconductor/2DEG interface. In one-dimensional junctions, the induced gap $\Delta=\Delta_0\frac{\Gamma}{\Gamma+\Delta_0}$ depends on the broadening of Andreev levels within the semiconductor[38] $\Gamma=\frac{\hbar v_F}{L_{eff}}D_1D_2$, where we introduce contacts transparencies D_1 and D_2. We assume for simplicity that $D_1=D_2=1/(1+Z^2)$, where $0<Z<\infty$ is a interface barrier strength introduced in ref. 39, and Bagwell's effective channel length $L_{eff}=L+2\xi_0$. Using NbN superconducting gap, $\Delta_0=2.02k_BT_c^0$ (NbN is a strong-coupling superconductor, $T_c^0=11$ K) and $T_c=0.3$ K for R^B_{3-4} we obtain $Z=0.2$. This value is consistent with the fit of the I_c versus T-dependence with D as a free parameter (Supplementary Fig. 2; Supplementary Note 2). Similar values of Z can be estimated from the analysis of the shape of dI/d$V(V)$ characteristics at elevated temperatures, as shown in Fig. 3. At $T<T_c^0$, Andreev reflection at S–2DEG interfaces results in an excess current flowing through the junction for voltage biases within the superconducting gap Δ_0/e and corresponding reduction of a differential resistance dV/dI by a factor of 2. In the presence of a tunnelling barrier, normal reflection competes with Andreev reflection and reduced excess current near zero bias, resulting in a peak in differential resistance. Within the Blonder–Tinkham–Klapwijk theory[39], a flat dV/d$I(V)$ within Δ_0/e, observed in our experiments, is expected only for contacts with very high transparency $Z<0.2$. For larger $Z>0.2$, a peak at low biases is expected (Supplementary Fig. 3, Supplementary Note 3). Several features of the experimental $I(V)$ need to be mentioned. First, we observe several sharp peaks in the resistance at high biases (around 2 and 4 mV for $T=4$ K). Similar sharp resonances has been observed previously[40], where authors attributed their appearance to the formation of Fabry–Pérot resonances between superconducting contacts. In our devices, the superconducting region is shunted by a low resistance ($<100\,\Omega$) 2DEG, thus appearance of $>10\,\mathrm{k}\Omega$ resonances cannot be explained by resonant electron trapping between contacts. These resonances are also observed in $I(V)$ characteristics of a single S–2DEG interface (measured in the S–2DEG–N configuration between contacts 3 and 6, see Supplementary Fig. 3). Differential resistance does not change substantially across resonances, ruling out transport through a localized state. We speculate that in the contacts where these resonances are observed superconductivity is carried out by quasi-one-dimensional channels, and jumps in I/V characteristics are due to flux trapping at high currents. This scenario is consistent with the observation that peaks shift to lower currents at higher fields, see Fig. 4. The second notable feature of our data is reduction of the zero-bias resistance by ≈ 2.6 times at low temperatures, while Andreev reflection limits the reduction to the factor of 2. We attribute this reduction to the multiple Andreev reflection between two closely spaced contacts, for contacts with larger separation (20 μm) multiple Andreev reflection is suppressed and the reduction of resistance by a factor of 2 is observed (Supplementary Fig. 3).

Induced superconductivity in low magnetic fields. Finally, we present magnetic field dependence of induced superconductivity. The low-field data is shown in Fig. 4a,b, where black regions

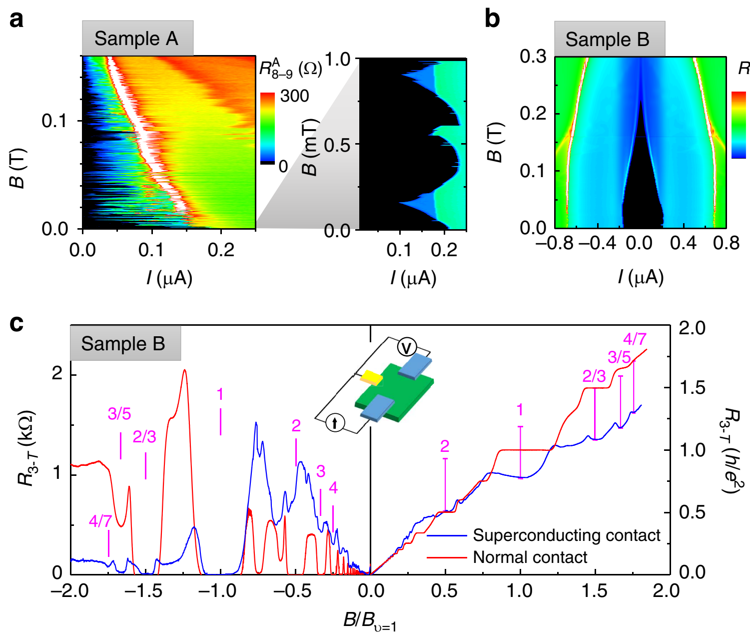

Figure 4 | Magnetic field dependence of induced superconductivity. (**a**,**b**) Differential resistance is measured as a function of B and $I_{d.c.}$ for two samples at 40 mK. Induced superconductivity (black region) is observed up to 0.2 T in both the samples. (**c**) 3-terminal resistance for a sample with all normal contacts (red) and between normal and superconducting contacts in sample B (I (2-4) and V (4 – 1) in Fig. 1) is measured at 70 and 40 mK, respectively. $B<0$ ($B>0$) induces clockwise (counterclockwise) chiral edge channels, note resistance scales difference for two field directions.

correspond to zero-differential resistance. Induced superconductivity is suppressed at ≈ 0.2 T in both the samples. In sample A, a narrow region of a 2DEG with induced superconductivity is confined between large NbN superconducting leads with rigid phases. Perpendicular magnetic field twists the phase in the 2DEG resulting in Fraunhofer-like oscillations of the critical current. In this sample, although the 2DEG extends beyond the narrow region between the contacts and I_c does not decrease to zero and abrupt jumps in I_c reflect multiple flux jumps. The period of oscillations is ~ 0.5 mT, which corresponds to an area of 4.1 μm^2, much smaller than the area of the 2DEG between the contacts ($\approx 120\, \mu m^2$). This observation is consistent with the reduced I_cRN product measured for this sample as discussed above. In sample B, contacts are fabricated along the edge of the mesa and 2D gas is not enclosed between the contacts. Consequently, I_c is a smooth function of B.

Superconductivity and quantum Hall effect. Competition between superconductivity and chiral quantum Hall edge states is shown in Fig. 4c, where resistance is measured in a 3-terminal configuration over a wide range of magnetic fields. Simple Landauer–Büttiker model of edge states predicts zero resistance for negative and quantized Hall resistance for positive field direction for integer QHE and fractional QHE states, which is clearly seen in a sample with non-superconducting (AuGe) ohmic contacts (red curve). When a superconducting contact serves as a current injector (blue curve), integer $\nu=1$ and fractional $\nu=2/3$ and 3/5 states are well developed for $B<0$, while the same states are not quantized at proper QHE values for $B>0$. If we assume that current injection via a superconducting contact results in an extra voltage offset at the contact by $V_{off} \approx \Delta_{ind}/e$, the measured voltage will be reduced by V_{off}. The magenta bars for $B>0$ indicate corrected resistance $(V-V_{off})/I$ for $V_{off}=140\, \mu V$. While this offset may explain the measured values for fractional states, a twice smaller V_{off} is needed to reconcile the resistance at $\nu=1$. Note that NbN critical field $B_c>16$ T. At low fields, states $\nu=3$, 4 and 5 have resistance minima for $B<0$, indicating a partial equilibration of chiral edge currents with the superconducting contact, while resistance near $\nu=2$ has a maximum. Zero resistance at $\nu=1$ and large resistance at $\nu=2$ are in contrast to the theoretical prediction that $\nu=2$ state should be stronger coupled with a superconducting contact than $\nu=1$ (ref. 23).

Methods

GaAs wafers design and parameters. The GaAs/AlGaAs inverted heterojunctions were grown by molecular beam epitaxy on semi-insulating (100) GaAs substrates with the heterointerface placed 130 nm below the surface and δ-doping layer 30–40 nm below the GaAs/AlGaAs interface. Samples were fabricated from two wafers with density and mobility $n=2.7\times10^{11}\,cm^{-2}$, $\mu=2\times10^{6}\,V\,s\,cm^{-2}$ (sample A) and $n=1.7\times10^{11}\,cm^{-2}$, $\mu=4\times10^{6}\,V\,s\,cm^{-2}$ (sample B).

Fabrications of superconducting contacts. Superconducting contacts were defined by standard electron beam lithography. First, a 120 nm—deep trench was created by wet etching. Next, samples were dipped into HCl:H_2O (1:6) solution for 2 s and loaded into a thermal evaporation chamber, where Ti/AuGe (5/50 nm) was deposited. Finally, 70 nm of NbN was deposited by DC magnetron sputtering in Ar/N_2 (85/15%) plasma at a total pressure of 2 mTorr. Deposition conditions were optimized for producing high quality NbN films with $T_c=11$ K and $B_c>15$ T, see Supplementary Fig. 4, and with minimal strain[41]. After metallization, contacts were annealed at 500 °C for 10 min in a forming gas (10% H_2 in Ar). Measurements were performed in a dilution refrigerator with the base temperature <30 mK, high-temperature data was obtained in a variable temperature ^{3}He system. Samples were illuminated with red light-emitting diode at 4 K to form a 2D gas, 2-terminal resistance drops from $>1\,M\Omega$ before illumination to $<500\,\Omega$ after illumination.

References

1. Clark, T. D., Prance, R. J. & Grassie, A. D. C. Feasibility of hybrid Josephson field effect transistors. *J. Appl. Phys.* **51,** 2736–2743 (1980).
2. Takayanagi, H. & Kawakami, T. Superconducting proximity effect in the native inversion layer on InAs. *Phys. Rev. Lett.* **54,** 2449–2452 (1985).
3. Akazaki, T., Takayanagi, H., Nitta, J. & Enoki, T. A Josephson field effect transistor using an InAs inserted channel $In_{0.52}Al_{0.48}As/In_{0.53}Ga_{0.47}$ As inverted modulation-doped structure. *Appl. Phys. Lett.* **68,** 418–420 (1996).
4. Heersche, H. B., Jarillo-Herrero, P., Oostinga, J. B., Vandersypen, L. M. K. & Morpurgo, A. F. Bipolar supercurrent in graphene. *Nature* **446,** 56–59 (2007).
5. Sacepe, B. *et al.* Morpurgo. Gate-tuned normal and superconducting transport at the surface of a topological insulator. *Nat. Commun.* **2,** 575 (2011).

6. Williams, J. R. *et al.* Unconventional Josephson effect in hybrid superconductor-topological insulator devices. *Phys. Rev. Lett.* **109,** 056803 (2012).
7. Veldhorst, M. *et al.* Josephson supercurrent through a topological insulator surface state. *Nat. Mater.* **11,** 1–4 (2012).
8. Qu, F. *et al.* Strong superconducting proximity effect in Pb-Bi_2Te_3 hybrid structures. *Sci. Rep* **2,** 339 (2012).
9. Doh, Y.-J. *et al.* Tunable supercurrent through semiconductor nanowires. *Science* **309,** 272–275 (2005).
10. Jarillo-Herrero, P., van Dam, J. A. & Kouwenhoven, L. P. Quantum supercurrent transistors in carbon nanotubes. *Nature* **439,** 953–956 (2006).
11. Xiang, J., Vidan, A., Tinkham, M., Westervelt, R. M. & Lieber., C. M. Ge/Si nanowire mesoscopic Josephson junctions. *Nat. Nanotechnol.* **1,** 208–213 (2006).
12. Hart, S. *et al.* Induced superconductivity in the quantum spin hall edge. *Nat. Phys.* **10,** 638–643 (2014).
13. Yu, W. *et al.* Superconducting proximity effect in inverted InAs/GaSb quantum well structures with Ta electrodes. preprint at arXiv:1402.7282 (2014).
14. Rokhinson, L. P., Liu, X. & Furdyna., J. K. The fractional a.c. Josephson effect in a semiconductor-superconductor nanowire as a signature of Majorana particles. *Nat. Phys.* **8,** 795–799 (2012).
15. Mourik, V. *et al.* Signatures of Majorana fermions in hybrid superconductor-semiconductor nanowire devices. *Science* **336,** 1003–1007 (2012).
16. Fu, L. & Kane, C. L. Josephson current and noise at a superconductor/quantum-spin-Hall-insulator/superconductor junction. *Phys. Rev. B* **79,** 161408 (2009).
17. Lutchyn, R. M., Sau, J. D. & Sarma, S. D. Majorana fermions and a topological phase transition in semiconductor-superconductor heterostructures. *Phys. Rev. Lett.* **105,** 077001 (2010).
18. Alicea, J. Majorana fermions in a tunable semiconductor device. *Phys. Rev. B* **81,** 125318 (2010).
19. Clarke, D. J., Alicea, J. & Shtengel, K. Exotic non-Abelian anyons from conventional fractional quantum Hall states. *Nat. Commun.* **4,** 1348 (2012).
20. Mong, R. S. K. *et al.* Universal topological quantum computation from a superconductor-Abelian quantum hall heterostructure. *Phys. Rev. X* **4,** 011036 (2014).
21. Zuo, Z.-W., Sheng, L. & Xing., D. Y. Crossed Andreev reflections in superconductor and fractional quantum Hall liquids hybrid system. *Solid State Commun.* **184,** 17–20 (2014).
22. Zyuzin, A. Y. Superconductor-normal-metal-superconductor junction in a strong magnetic field. *Phys. Rev. B* **50,** 323–329 (1994).
23. Fisher., M. P. A. Cooper-pair tunneling into a quantum Hall fluid. *Phys. Rev. B* **49,** 14550–14553 (1994).
24. Hoppe, H., Zülicke, U. & Schön, G. Andreev reflection in strong magnetic fields. *Phys. Rev. Lett.* **84,** 1804–1807 (2000).
25. Kim, E.-A., Vishveshwara, S. & Fradkin., E. Cooper-pair tunneling in junctions of singlet quantum Hall states and superconductors. *Phys. Rev. Lett.* **93,** 266803 (2004).
26. Giazotto, F., Governale, M., Zülicke, U. & Beltram, F. Andreev reflection and cyclotron motion at superconductor/normal-metal interfaces. *Phys. Rev. B* **72,** 054518 (2005).
27. van Ostaay, J. A. M., Akhmerov, A. R. & Beenakker, C. W. J. Spin-triplet supercurrent carried by quantum Hall edge states through a Josephson junction. *Phys. Rev. B* **83,** 195441 (2011).
28. Lenssen, K-M. H. *et al.* Andreev reflection at superconducting contacts to GaAs/AlGaAs heterostructures. *Appl. Phys. Lett.* **63,** 2079–2081 (1993).
29. Moore, T. D. & Williams, D. A. Andreev reflection at high magnetic fields. *Phys. Rev. B* **59,** 7308–7311 (1999).
30. Verevkin, A. A. *et al.* Multiple Andreev reflection in hybrid AlGaAs GaAs structures with superconducting NbN contacts. *Semiconductors* **33,** 551–554 (1999).
31. Takayanagi, H., Akazaki, T., Kawamura, M., Harada, Y. & Nitta, J. Superconducting junctions using AlGaAs/GaAs heterostructures with high h_{c2} NbN electrodes. *Physica E* **4,** 922–926 (2002).
32. Kutchinsky, J., Taboryski, R., Srensen, C. B., Hansen, J. B. & Lindelof, P. E. Experimental investigation of supercurrent enhancement in s-n-s junctions by non-equilibrium injection into supercurrent-carrying bound Andreev states. *Physica C* **352,** 4–10 (2001).
33. Marsh, A. M., Williams, D. A. & Ahmed, H. Supercurrent transport through a high-mobility two-dimensional electron gas. *Phys. Rev. B* **50,** 8118–8121 (1994).
34. Tan, I.-H., Snider, G. L., Chang, L. D. & Hu., E. L. A self-consistent solution of schrodinger-poisson equations using a nonuniform mesh. *J. Appl. Phys.* **68,** 4071 (1990).
35. Kulik, I. O. & Omel'anchuk, A. N. Properties of superconducting microbridges in the pure limit. *Sov. J. Low Temp. Phys.* **3,** 459–461 (1977).
36. Kulik, I. O. & Omel'yanchuk, A. N. Contribution to the microscopic theory of the Josephson effect in superconducting bridges. *Sov. Phys. JETP* **21,** 96–97 (1975).
37. Bagwell, P. F. Suppression of the Josephson current through a narrow, mesoscopic, semiconductor channel by a single impurity. *Phys. Rev. B* **46,** 12573–12586 (1992).
38. Sau, J. D., Tewari, S. & Sarma, S. D. Experimental and materials considerations for the topological superconducting state in electron and hole doped semiconductors: searching for non-Abelian Majorana modes in 1d nanowires and 2d heterostructures. *Phys. Rev. B* **85,** 064512 (2012).
39. Blonder, G. E., Tinkham, M. & Klapwijk, T. M. Transition from metallic to tunneling regimes in superconducting microconstrictions: excess current, charge imbalance, and supercurrent conversion. *Phys. Rev. B* **25,** 4515–4532 (1982).
40. Gao, J. R. *et al.* Superconductors coupled with a two-dimensional electron gas in GaAs/AlGaAs and InAs/AlGaSb heterostructures. *Surf. Sci.* **305,** 470–475 (1994).
41. Glowacka, D. M. *et al.* Development of a NbN deposition process for superconducting quantum sensors. preprint at arXiv:1401.2292 (2014).

Acknowledgements

The work at Purdue was supported by the National Science Foundation grant DMR-1307247 (Z.W. and L.P.R.), by the Purdue Center for Topological Materials (Z.W.) and by the US Department of Energy, Office of Basic Energy Sciences, Division of Materials Sciences and Engineering under Awards DE-SC0008630 (A.K.) and DE-SC0006671 (M.J.M.). The work at Princeton was funded by the Gordon and Betty Moore Foundation through Grant GBMF 4420 and by the National Science Foundation MRSEC at the Princeton Center for Complex Materials.

Author contributions

L.P.R. and M.J.M conceived the experiments, Z.W. fabricated samples, Z.W. and L.P.R performed the experiments, Z.W. and L.P.R wrote the manuscript with comments from M.J.M, L.N.P. and K.W.W. designed and grew wafers, and A.K. contributed to the fabrication and low temperature experiments.

Additional information

Supplementary Information accompanies this paper at http://www.nature.com/naturecommunications

Competing financial interests: The authors declare no competing financial interests.

Reprints and permission information is available online at http://npg.nature.com/reprintsandpermissions/

How to cite this article: Wan, Z. *et al.* Induced superconductivity in high-mobility two-dimensional electron gas in gallium arsenide heterostructures. *Nat. Commun.* 6:7426 doi: 10.1038/ncomms8426 (2015).

SUPPLEMENTARY FIGURES

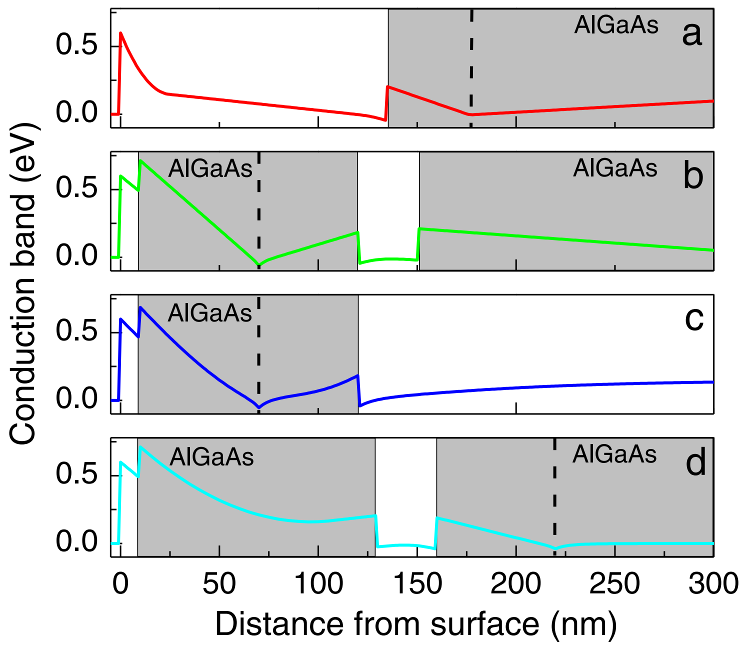

Supplementary Figure 1. **Comparison between conventional heterostructure and inverted single interface heterojunction.** Conduction band profile is plotted for (a) inverted single interface heterojunction used in our experiments and typical (b) modulation-doped quantum well, (c) single heterojunction, and (d) inverted quantum well. Dash lines indicate position of modulation doping.

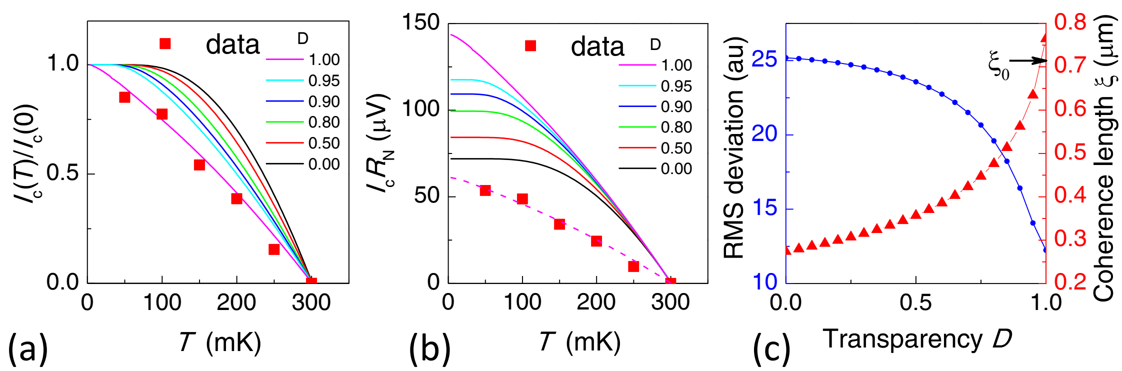

Supplementary Figure 2. **Analysis of the temperature dependence of the critical current.** Scaled (a) and unscaled (b) product I_cR_N is calculated using Eq. (1) for different transparencies D and $\alpha = 1$. Red dots are experimental data. Dashed line in (b) is for $\alpha = 0.7$ and $D = 1$. In (c) root-mean-square deviation between the best fit and the experimental data is shown for different D, coherence length ξ obtained from the best fit are red triangles.

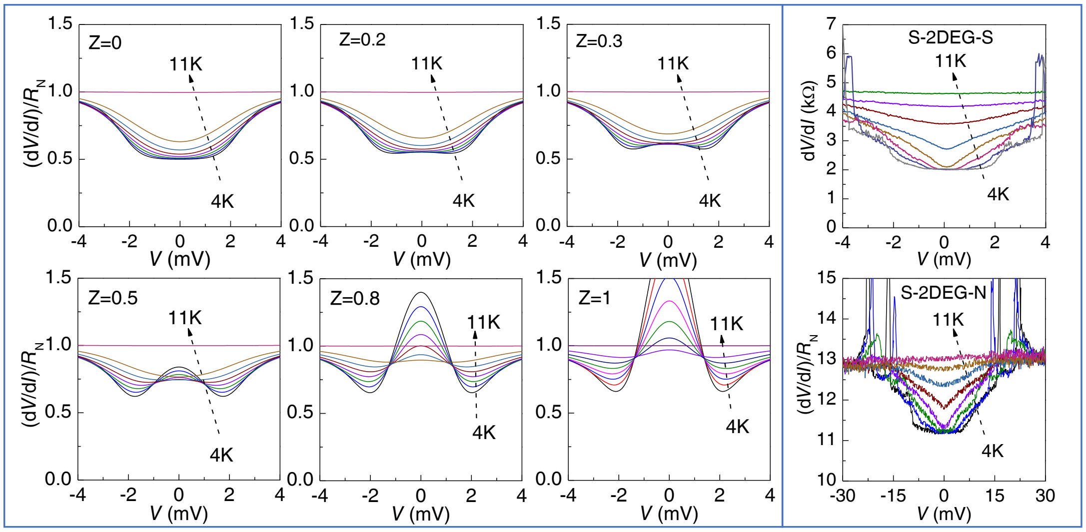

Supplementary Figure 3. **Temperature dependence of differential resistance.** Left 6 plots: normalized differential resistance is calculated using BKT theory, Eq. 2, for different barriers Z and temperatures between 4 and 11 K with a step of 1 K. Right 2 plots: experimentally measured differential resistance between two superconducting contacts (R_{3-5}) and a normal-superconducting contact (R_{4-7}) in sample B (the normal contact has high resistance).

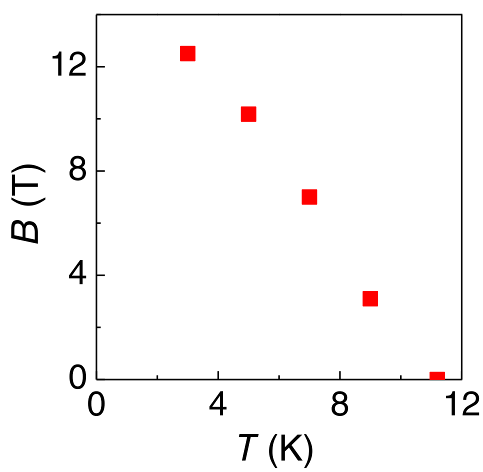

Supplementary Figure 4. **Temperature dependence of the NbN critical field.** Critical field of a 40 nm NbN film sputtered with optimal conditions is measured as a function of temperature.

SUPPLEMENTARY NOTES

Supplementary Note 1. Comparison between conventional heterostructures and an inverted single interface heterojunction

Comparison between conventional heterostructures and inverted single heterointerface structures used in this work is shown in Supplementary Figure 1. In conventional quantum well (b,d) and single interface heterostructures AlGaAs barrier between 2D gas and the surface adds 0.3 eV to the Schottky barrier if contacts are defused from the surface. For side contacts inverted single heterointerface (a) increases the exposed GaAs cross section for Cooper pair injection.

Supplementary Note 2. Temperature dependence of the critical current

Haberkorn et al. [1] generalized Kulik-Omelyanchuk current-phase relations[2, 3] to the case of arbitrary transparency of a tunnel barrier D inserted into the Josephson junction by directly solving Gor'kov's equations. They obtain the following current-phase relation:

$$I_{\rm s}(\phi, T)R_{\rm N} = \alpha\frac{\pi\Delta(T)}{2e}\frac{\sin(\phi)}{\sqrt{1 - D\sin^2(\phi/2)}} \times \tanh\frac{\Delta(T)}{2k_{\rm B}T}\sqrt{1 - D\sin^2(\phi/2)}, \qquad (1)$$

where $\Delta(T)$ is the BCS gap. For $\alpha = 1$ this equation interpolates between diffusive ($D = 0$) and ballistic ($D = 1$) junctions. Critical current can be found as $I_{\rm c}(T)R_{\rm N} = max[I_{\rm s}(\phi, T)R_{\rm N}]$. We introduce coefficient α to account for the reduction of the critical current due to the finite length of the junction L, $\alpha = 2\xi/(L+2\xi)$ [4]. The best fit to the experimental $I_{\rm c}R_{\rm N}(T)$ dependence assuming both α and D as free parameters is obtained for $D = 1$ and $\alpha = 0.7$, see Fig. 2(a,b). For the contact spacing $L = 0.63$ μm this α corresponds to $\xi = 0.76$ μm, consistent with the BCS coherence length $\xi_0 = \hbar v_{\rm F}/\pi\Delta = 0.72$ μm. Transparency D can be related to the dimensionless barrier strength Z introduced in the Blonder-Tinkham-Klapwijk (BTK) theory[5], $D = 1/(1 + Z^2)$, and the fit sets the upper limit on Z, $Z < 0.1$. The quality of the fit parameters can be assessed from Fig. 2(c), where RMS error for the best fit with a fixed D and α as a free parameter (RMS deviation)^2 = $\sum_i\{[I_{\rm c}(T_i)R_{\rm N}]^{theory} - [I_{\rm c}(T_i)R_{\rm N}]^{exp}\}^2$ is plotted for different D. The RMS deviation has a clear global minimum at $D \to 1$. Note that the coherence length for $D < 1$, obtained from the fitting parameter α, becomes smaller than the estimated ξ_0.

Supplementary Note 3. Analysis of excess current above the induced superconductivity gap

Transparency of the superconductor-semiconductor interface can be estimated from the shape of the $dV/dI(V)$ characteristic, where competition between Andreev and normal reflections results in a peak in differential resistance when a tunneling barrier is present at the superconductor-semiconductor interface (transmission $D = 1/(1 + Z^2) < 1$). Differential resistance for different temperatures can be calculated using Blonder-Tinkham-Klapwijk (BTK) theory[5]:

$$\frac{dI}{dV}(V) \propto \int_{-\infty}^{\infty} \frac{\partial f_0(E-eV)}{\partial(eV)}[1+A(E)-B(E)]dE, \quad (2)$$

where $f_0(E)$ is the Fermi Dirac function and $A(E)$ and $B(E)$ are energy-dependent Andreev and normal reflection coefficients, respectively. Both coefficients depend on the gap of NbN $\Delta_0 = \Delta(T)$ with $T_c^0 = 11$ K and the interface barrier strength Z. In Supplementary Figure. 3 we plot differential resistance for different values of Z. At low T for $Z = 0$ the barrier is transparent ($D = 1$) and all incident electrons are Andreev reflected, which leads to the a reduction of differential resistance by a factor of 2 within the energy gap Δ_0. When Z is finite, part of the incident electrons undergoes normal reflection which results in the increase of the resistance within the gap.

The exact shape of experimental curves differ from the shape predicted by the BKT theory, the most important deviation being sharp minima near $V = 0$ observed at T close to T_c^0 as compared to a much smoother BKT dependence. To account for a similar sharpening of a zero-bias peak in less transparent contacts ($Z > 2$) it has been assumed that a thin normal region is formed between NbN contacts and a 2DEG[6]. This more elaborate theory introduces two more fitting parameters for the superconducting-normal and normal-2DEG interfaces, but does not change the main qualitative prediction of a simpler BTK theory: appearance of a peak near $V = 0$ for $Z > 0.2$ in $dV/dI(V)$ characteristics.

Experimentally, we observe no zero-bias peak in $dV/dI(V)$ characteristics measured between two superconducting contacts R_{3-4} (S-2DEG-S) or between superconducting and normal contacts R_{8-9} (S-2DEG-N), see Figure. 3 and Supplementary Figure 3, thus we can set an upper limit $Z < 0.2$ and lower limit $D > 0.96$ for our contacts.

SUPPLEMENTARY REFERENCES

[1] W. Haberkorn, H. Knauer, and J. Richter, "A theoretical study of the current-phase relation in Josephson contacts," Physics Status Solidi **47**, K161–K164 (1978).

[2] I.O. Kulik and A.N. Omel'yanchuk, "Properties of superconducting microbridges in the pure limit." Soviet Journal of Low Temperature Physics **3**, 459 – 461 (1977).

[3] I.O. Kulik and A.N. Omel'yanchuk, "Microscopic theory of the Josephson effect in superconducting bridges," Pisma v ZETF **21**, 216 – 19 (1975).

[4] Philip F. Bagwell, "Suppression of the Josephson current through a narrow, mesoscopic, semiconductor channel by a single impurity," Phys. Rev. B **46**, 12573–12586 (1992).

[5] G. E. Blonder, M. Tinkham, and T. M. Klapwijk, "Transition from metallic to tunneling regimes in superconducting microconstrictions: Excess current, charge imbalance, and supercurrent conversion," Phys. Rev. B **25**, 4515–4532 (1982).

[6] K. Neurohr, A. A. Golubov, Th. Klocke, J. Kaufmann, Th. Schäpers, J. Appenzeller, D. Uhlisch, A. V. Ustinov, M. Hollfelder, H. Lüth, and A. I. Braginski, "Properties of lateral Nb contacts to a two-dimensional electron gas in an $In_{0.77}Ga_{0.23}As/InP$ heterostructure," Phys. Rev. B **54**, 17018–17028 (1996).